

## **Determining bathymetry of shallow and ephemeral desert lakes using satellite imagery and altimetry**

**M. Armon<sup>1</sup>, E. Dente<sup>1,2,3</sup>, Y. Shmilovitz<sup>1,2</sup>, A. Mushkin<sup>2</sup>, T. J. Cohen<sup>4</sup>, E. Morin<sup>1</sup>, and Y. Enzel<sup>1</sup>**

<sup>1</sup>The Fredy and Nadine Herrmann Institute of Earth Sciences, the Hebrew University of Jerusalem, Israel.

<sup>2</sup>The Geological Survey of Israel, Israel.

<sup>3</sup>Shamir Research Institute, University of Haifa, Israel.

<sup>4</sup>School of Earth and Environmental Sciences, University of Wollongong, Australia.

Corresponding author: Moshe Armon ([moshe.armon@mail.huji.ac.il](mailto:moshe.armon@mail.huji.ac.il))

### **Key Points:**

- A new methodology to produce bathymetry maps of shallow desert lakes was developed, based on globally available datasets
- The methodology enables mapping the bathymetry of lakes with sub-basins or partially flooded lakes; both major limitations of other methods
- The derived bathymetry error is ~30 cm, rather than ~2.5 m for other globally available data

## 1 **Abstract**

2 Water volume estimates of shallow desert lakes are the basis for water balance calculations,  
3 important both for water resource management and paleohydrology/climatology. Water volumes  
4 are typically inferred from bathymetry mapping; however, being shallow, ephemeral and remote,  
5 bathymetric surveys are scarce in such lakes. We propose a new, remote-sensing based, method  
6 to derive the bathymetry of such lakes using the relation between water occurrence, during >30-  
7 yr of optical satellite data, and accurate elevation measurements from the new Ice, Cloud, and  
8 Land Elevation Satellite-2 (ICESat-2). We demonstrate our method at three locations where we  
9 map bathymetries with ~0.3 m error. This method complements other remotely sensed,  
10 bathymetry-mapping methods as it can be applied to: (a) complex lake systems with sub-basins,  
11 (b) remote lakes with no in-situ records, and (c) flooded lakes. The proposed method can be  
12 easily implemented in other shallow lakes as it builds on publically accessible global data sets.

## 13 **Plain Language Summary**

14 Lakes in desert environments are often remote, shallow, and only get filled once in a long while.  
15 They are an important water resource, and could be used to decipher past environmental  
16 conditions. However, detailed maps of lake-floor terrain, which are required to effectively study  
17 these lakes are typically not available. The deepest parts of the lakes are filled with water more  
18 frequently than their shallow margins. Thus, we suggest here to relate water occurrence in those  
19 lakes with accurate satellite-based elevation measurements, to obtain a valuable lake-floor terrain  
20 map. We demonstrate the usefulness of our method by comparing results with other globally  
21 available data. Previous methods struggle with complex-terrain lakes or lakes that are partially  
22 flooded during their survey; while our method yields high-resolution accurate maps even in such  
23 lakes.

## 24 **1 Introduction**

25 A major characteristic of drylands is endoreism, internal drainage (de Martonne, 1927). The lower and usually drier  
26 parts of these drylands are often occupied by ephemeral or seasonal shallow desert lakes (Nicholson, 2011).  
27 Thousands of such lakes exist globally with the largest being Lake Eyre (Australia, alias Kati Thanda; surface area  
28 of >9000 km<sup>2</sup> when full). Such lakes are significant for opportunistic species that have no other water resources  
29 (e.g., D'Odorico and Porporato, 2006; Noy-Meir, 1973). Mapping of lake floors is key in calculating water balance  
30 (e.g., Cohen et al., 2015; Enzel and Wells, 1997), important in water resources management, and in deciphering  
31 paleohydrology (e.g., Crétaux et al., 2016; Quade et al., 2018). However, being shallow, dry and remote,  
32 bathymetric surveys (e.g., as in Bye et al., 1978) have been scarce in such lakes.

33 A different approach to bathymetry mapping is through remote-sensing (Gao, 2015; Jawak et al., 2015). The Shuttle  
34 Radar Topography Mission (SRTM) has provided high resolution (~30m) global digital elevation models (DEMs)  
35 that could, in principal, present bathymetry of such desert lakes. Yet, radar altimetry cannot produce accurate DEMs  
36 if the area is flooded or where lake floors are exceptionally bright and/or smooth (Berry et al., 2007; Brenner et al.,  
37 2007), which are common conditions.

38 To improve lake-bathymetry maps, recent studies either integrate remote-sensing data with a spatial interpolation of  
39 in-situ measurements (Feng et al., 2011; Leon and Cohen, 2012) or combine between optical imaging and radar  
40 (e.g., Sun and Ma, 2019) or laser altimetry (Arsen et al., 2013; Li et al., 2019; Ma et al., 2019). These satellite  
41 imaging methods are based on determining isobaths (equal depth lines) of a lake, through snapshots during different  
42 lake stages. Then, shorelines in each specific image are assigned a height through accurate elevation measurements;  
43 such as laser altimetry. This determines bathymetry only to the depth of the lowest shoreline identified, using a  
44 spatial interpolation of a few isobaths. It also overlooks the possible variance in elevation of a specific shoreline,  
45 which can be significant in large lakes (Arsen et al., 2013; Feng et al., 2011). Li et al. (2019) suggested using a long-  
46 term (410 images during >30-yr) water occurrence index, instead of a few specific isobaths, and relating it with  
47 measurements from a limited dataset of airborne lidar altimetry. This overcomes shoreline elevation variations and

48 makes spatial interpolation unnecessary. However, they assumed a linear relation between isobath areas, sampled at  
49 specific points, and elevation. Applying their methodology to a deep reservoir (Lake Mead; >100m deep) only  
50 revealed the bathymetry of the upper part of the lake; the deeper bathymetry was extrapolated with geometrical  
51 considerations, calibrated using in-situ data (Li et al., 2019). A further complication arises where water occurrence is  
52 not based directly on elevation, primarily where a lake is composed of a few sub-basins, which yields more than one  
53 possible relation between water occurrence and elevation. Accordingly, present-day methodologies and freely  
54 available datasets cannot provide accurate, high-resolution bathymetry of often-flooded, shallow desert lakes,  
55 especially for lakes having more than one sub-basin.

56 Thus, to derive the bathymetry of desert lakes, there is a need for: (a) an efficient and reliable way to recognize the  
57 water occurrence at a high resolution, (b) a technique to overcome diverse water occurrences-elevation relations in  
58 different sub-basins, (c) a way to derive the bathymetry when lakes are inundated, and (d) a robust method to  
59 validate the resultant bathymetry. To tackle these challenges, we developed a simple and easily implemented  
60 methodology that derives bathymetry of shallow desert lakes. This paper focuses on three desert lakes, ranging in  
61 area from  $0.2 \times 10^3 \text{ km}^2$  to  $6 \times 10^3 \text{ km}^2$ . Lake bathymetries are acquired using the relation between globally-available  
62 high-resolution (30 m) water occurrence maps, and elevation data from NASA's new Ice, Cloud, and Land  
63 Elevation Satellite-2 (ICESat-2).

64 Following is a description of the methodology and its application over Lake Eyre, which consists of a few sub-  
65 basins. We show the derivation of a bathymetric map for the lake and validate it versus the global SRTM and the  
66 best bathymetric map available for the region (Section 3). Having better results than the SRTM, we set to derive the  
67 bathymetry of a remote lake in the Sahara (Sabkhat El-Mellah) that has no other bathymetric map (Section 4) and of  
68 Lago Coipasa in the Altiplano for which we separately derive the bathymetry under dry and inundated conditions.

## 69 **2 Methodology**

70 Desert lakes are often fed by floods with monthly to decadal frequencies. Most of the coarser particles are deposited  
71 upstream, and thus, lake floors are mainly covered with fine low-permeability sediments, making evaporation the  
72 primary output (Nicholson, 2011). Water occurrence in these lakes is <100% of the time, and often <30%. Thanks to  
73 a detailed analysis of  $3 \times 10^6$  Landsat images by Pekel et al. (2016), the frequency of water occurrence over 30 m  
74 pixels between 1984 and 2015 is easily accessible worldwide. Water occurs more often over the deeper parts of the  
75 lake, where complete evaporation takes longer, and less often over the higher lake margins. Thus, there should be a  
76 straightforward relation between water occurrences (i.e., the relative frequency of water in a pixel) and lake floor  
77 elevation over such lakes. This, in turn, allows measuring height over specific locations within the lake, from which  
78 we can infer the entire lake floor elevation.

79 ICESat-2 provides dense and accurate elevation measurements (0.7 m point spacing; accuracy and precision of <5  
80 cm and <13 cm, respectively) over land, and even underwater. Thus it yields accurate, narrow (~14m) height  
81 profiles of Earth surface, since its launch in September 2018, with a 91-day revisiting frequency (Brunt et al., 2019;  
82 Markus et al., 2017). Underwater measurements can penetrate up to ~1 Secchi depth (Parrish et al., 2019), i.e. up to  
83 a few meters or even a few dozens of meters (Ma et al., 2019), depending on the optical properties of the water.

84 To derive bathymetry maps we rely on the relation between Water Occurrence and Laser Profile elevation (hereon  
85 WOLP) using four (to five) steps (described schematically in the supporting information Figure 1 [S1]): (a)  
86 acquiring a lake water occurrence map from the global water occurrence (Pekel et al., 2016); (b) extracting ICESat-2  
87 elevation data (ATL03 product) that coincide with the lake (defined as regions with >0% water occurrence) (Figure  
88 1a); (c) fitting a mathematical function describing the relation between water occurrence values and elevations  
89 (Figure 1b) based on all available scans in the lake extent; and (d) applying the fitted function areally, to translate  
90 the water occurrence map into lake-floor elevation over the entire lake basin (Figure 1d). For lakes consisting of  
91 sub-basins, an additional step is needed between steps c and d, in which we identify lake sub-basins from water  
92 occurrence, as detailed in Section 3 (e.g., Figure 1c). This methodology provides a bathymetric map of lakes that  
93 were flooded to some extent between 1984 and 2015, with a resolution of ~30 m.

94 To evaluate our methodology, we use available topographic data to demonstrate differences between our results and  
95 available bathymetric (or topographic) maps. Where the SRTM is the best external source, we use cross-validation,  
96 putting aside one ICESat-2 scan each time and validating the bathymetry based on all other scans. Owing to the high  
97 accuracy of the ICESat-2 data, we demonstrate the small expected error using our methodology.  
98

### 99 **3 Lake Eyre**

100 Lake Eyre (Figure 2c, e) has a watershed covering almost 1% of the global land area ( $>1.1 \times 10^6$  km<sup>2</sup>). It has a  
 101 complex lake floor with a minimum elevation of -15.2 m relative to the Australian Height Datum (AHD) (Kotwicki  
 102 and Isdale, 1991). The great flood of 1974 was utilized to perform bathymetric surveys over the lake, yielding a 0.5-  
 103 m-contour-interval bathymetric map and detailing features  $>1$  km<sup>2</sup> (Bye et al., 1978). Leon & Cohen (2012) (hereon  
 104 LC12) combined data from this bathymetric map with SRTM data and ICESat-1 laser altimetry (with 170 m point  
 105 spacing) to form the best bathymetric map of the lake that we are aware of. Because of its vast size, complex  
 106 bathymetry, and a good reference map, we chose to apply our methodology over Lake Eyre. To have a continuous  
 107 map, we only mapped Lake Eyre North (the larger and more frequently flooded part of the lake).  
 108 To overcome complexity arising from the different relations of water occurrence and elevation in each of the sub-  
 109 basins (Figure 1b), we divided Lake Eyre North into five sub-basins using the water occurrence map (Figure 1a, S2).  
 110 This enabled identification of pseudo watersheds, similar to determining watersheds in a topographic map  
 111 (Supporting Information 1 [SI1]; Schwanghart and Scherler (2014)). We then performed steps b to d of our  
 112 methodology, separately for each sub-basin (as exemplified in Figure 1c). If more than one ICESat-2 scan intersected a  
 113 watershed, we used data from all available scans. To form a single map out of the different sub-basins, regions close  
 114 to the pseudo water divide were assigned values using step c from all neighboring sub-basins, inversely weighted  
 115 according to their distance from the divide (SI1).

116  
 117 We validated the WOLP bathymetry map (Figure 1d) against SRTM data and the LC12 bathymetry over the entire  
 118 region (Table 1, Figures 2a, 2b), and against ICESat-2 scans over the measured profiles (Figure S3). The WOLP  
 119 bathymetry lies within  $\pm 0.5$  m of LC12 elevations for 74% of the region (90% is within  $\pm 1$  m), i.e., it lies within one  
 120 elevation contour of Bye et al. (1978). Most of the remaining areas (deviating  $>1$  m) are situated next to the lake  
 121 margins, where the LC12 map is mostly based on SRTM data, which were acquired during a lake inundation  
 122 interval, and are therefore not reliable over major parts of the lake (Leon and Cohen, 2012). In  $\sim 83\%$  of the area  
 123 SRTM data were replaced by a constant elevation value (-15 m AHD). The root mean square difference (RMSD) of  
 124 the SRTM data versus the LC12 map is 1.77 m, and only 25% of the SRTM data are within  $\pm 0.5$  m of LC12,  
 125 whereas the WOLP bathymetry has a RMSD of 0.52 m (Table 1). Moreover, the mean RMSD for each of the sub-  
 126 basins using cross-validation of the different ICESat-2 scans is 0.21-0.57 m (Figure S4), indicating that the WOLP  
 127 map error is even smaller than it seems when comparing it to the LC12 map.  
 128 Hypsometric curves emphasize differences between these analyzed bathymetries (Figure 3), and are important for  
 129 water volume estimates (SI2). Whereas the SRTM wet area sharply increases above the minimum elevation, because  
 130 of the constant (-15 m) elevation polygon, the WOLP and the LC12 wet area curves present a gradual increase with  
 131 depth (Figure 3a). Accordingly, water volumes are lower by  $\sim 75\%$  both in the WOLP and LC12 bathymetries  
 132 compared to the SRTM. Both the WOLP and the LC12 exhibit similar hypsometry in depths of  $<1$  m (dissimilar to  
 133 the SRTM). According to these maps, the southwestern sub-basin (Belt Bay) is the first to be filled (in accordance  
 134 with MODIS imagery of floods, Supplementary movie 1 [SM1]). Differences between WOLP and LC12  
 135 bathymetries increase above lake depths of 1 m, when the southeastern sub-basin (Madigan Gulf) fills according to  
 136 WOLP bathymetry. In the LC12 map, the sill between the southern sub-basins is higher and therefore the flooded  
 137 area increases only above water depth of 2 m. Large differences exist between WOLP and LC12 at the lake's  
 138 margins; there, LC12 bathymetry rises  $\sim 5$  m above the lake bottom (Figure 3a). These differences seem to be related  
 139 to the SRTM-dependent mapping of the lake margins in LC12. At a depth of 3.1 m, the WOLP flooded area reaches  
 140 its maximum extent, featuring an area of  $6.1 \times 10^3$  km<sup>2</sup> and a volume of 8.9 km<sup>3</sup>,  $\sim 33\%$  higher than the respective  
 141 area and volume calculated based on the LC12 map (Figure 3a). Nevertheless, it is important to note that WOLP  
 142 bathymetry represents only regions that were flooded between 1984 and 2015, and that the largest flood in recent  
 143 history occurred in the 1970's. Therefore higher shorelines, as in LC12 or Cohen et al. (2018), could not be mapped  
 144 with WOLP.

145

### 146 **4 Application for non-mapped and inundated lakes**

147 Sabkhat El-Mellah is a small, northwestern Sahara ephemeral lake ( $\sim 170$  km<sup>2</sup>) (Figure 2e, f). It is fed in the High  
 148 Atlas Mountains and is flooded only once every few years (Mabbutt, 1977). There is no bathymetric map of this lake  
 149 that we are aware of. A comparison of the WOLP bathymetry (Figure S5) to the SRTM data (Figures 2d, S6)  
 150 indicates generally a similar pattern (location of the deepest part of the lake and its margins, large scale slopes, etc.).  
 151 However, variations of the SRTM data over Sabkhat El-Mellah are approximately  $\pm 2$  m (Figures 3b, S6), while lake

152 depth is ~5 m, yielding an uncharacteristic discontinuous and rough lake floor (e.g., Quade et al., 2018). The mean  
153 cross-validation RMSD of WOLP bathymetry is much lower (0.32 m; Table 1, Figure S7). The WOLP map exhibits  
154 a much higher flooded area in comparison with the SRTM data (Figure 3b). E.g., at a 1 m lake depth, the WOLP  
155 lake area is  $0.15 \times 10^3 \text{ km}^2$  versus  $0.08 \times 10^3 \text{ km}^2$  according to SRTM data.

156 The same methodology was applied over Lago Coipasa (or Salar de Coipasa; surface area up to  $2400 \text{ km}^2$ ), which is  
157 a high altitude (3660 m), shallow saline lake, occasionally filled with water (Placzek et al., 2006) (Figure 2e, i).  
158 However, during February 2019, the lake was flooded (SM2), thus, ICESat-2 scans taken afterward exhibit both the  
159 water surface and the lake floor in its inundated region.

160 Recent studies highlight the ability of ICESat-2 scans to penetrate water and yield bathymetric profiles (Forfinski-  
161 Sarkozi and Parrish, 2016; Ma et al., 2019; Parrish et al., 2019). Therefore, we derived two different bathymetric  
162 maps of Lago Coipasa, one using all available “dry” scans (i.e., before February 2019; Figure S8), and the other  
163 (Figure S9) using only post-flood scans (“wet” scans), manually omitting the ICESat-2’s water surface readings  
164 (SI3). The difference between the “dry” bathymetry and the SRTM data, and the difference between the “dry” and  
165 “wet” maps are shown in Figures 2g and 2h, respectively. Given the difficulty in determining water density, we did  
166 not correct the effect of the changing refraction coefficient between water and air on underwater elevation  
167 measurements. However, to avoid location errors, we used only nadir data, which are expected to have the least  
168 spatial error. The expected vertical error where water depth is ~0.7 m (SI3), as in this 2019 flood, is  $<0.18 \text{ m}$   
169 (Parrish et al., 2019) or even less (as shown in Ma et al., 2019).

170 Similar to Lake Eyre, the WOLP-SRTM difference map (Figure 2g) illustrates that Lago Coipasa was inundated  
171 during the SRTM scan, and the wet part of the scan was replaced with a fixed elevation value. The SRTM data over  
172 the lake area varies within  $\sim \pm 5 \text{ m}$  (RMSD=2.84 m; Figures 3c and S10), meaning that over a ~1.5 m deep lake, such  
173 as Lago Coipasa, SRTM-based water volume calculations for all practical matters are absurd. In contrast, both the  
174 “dry” and the “wet” WOLP bathymetries yield a much smaller mean cross-validation RMSD value (0.28 m and 0.47  
175 m, respectively; Table 1, Figures S11, S12).

176 The fixed-elevation polygon in the SRTM data for Lago Coipasa is bounded by high ( $>2 \text{ m}$ ) artificial walls. This is  
177 exhibited in the hypsometry by a sharp increase and then a fixed wetted area of  $0.87 \times 10^3 \text{ km}^2$  (Figure 3c). In lake  
178 depths of  $<1 \text{ m}$ , the “dry” bathymetry presents a detailed gradual increase in lake area and volume, filling most of  
179 the maximum lake extent. The “wet” WOLP area at 1 m depth is smaller than the “dry” area due to a 1.3 m deeper  
180 lake bottom in the “wet” bathymetry (Figure 3c; SI2). Both the “dry” and “wet” scans did not cross the northernmost  
181 part of the lake, which is characterized by the highest water occurrence (and presumably deepest water column). For  
182 this reason, we stress that future crossing of ICESat-2 over this specific region of the lake could improve its  
183 bathymetry.

184 Compared with the “dry” bathymetry, 58% of the “wet” lake area lies within  $\pm 0.5 \text{ m}$  of the “dry” bathymetry  
185 (RMSD = 0.39 m). Thus, relying on the “dry” bathymetric map, which seems reasonable in light of the results  
186 shown for Lake Eyre, we suggest that even when using only the “wet” scans, the WOLP bathymetry yields better  
187 results than the currently available global product (SRTM). This leads us to propose the usage of the methodology  
188 presented here for any of the world’s shallow desert lakes.

## 189 **5 Discussion**

190 The largest source of uncertainty in the WOLP bathymetry stems from the selected fitting equation between water  
191 occurrence and elevation (step c). However, this selection affects mainly the extremities of data, i.e., the  
192 extrapolation of elevation to values that were not observed by the ICESat-2 (areas with gray dots in Figures 1c, S5,  
193 S8, S9). Thus, in cases where ICESat-2 data covers the water frequency extremities, WOLP bathymetry is accurate,  
194 as demonstrated by the cross-validation results. Large enough lakes should be covered by at least a few ICESat-2  
195 scans (e.g., Figure 1a) and therefore, scans are expected to cover a wide range of water occurrences. This wide range  
196 can yield an accurate bathymetry for almost all of the lake extent.

197 Laser altimetry errors, estimated to be ~0.3 m for a single photon return, and much lower (0.05-0.07 m) for an  
198 average of neighboring photon returns (Jasinski et al., 2016), are not expected to impact our results significantly. A  
199 larger uncertainty lies between points that have a similar water occurrence but different elevation, as is the case if  
200 there are small and local topographic minima. Using more scans may decrease the variations, although some of them  
201 may be intrinsic, e.g., where transmission-losses or springs are common. Water occurrence minima can be too small  
202 to be identified as a different sub-basin. Thus, our method is limited to sub-basins that are large enough to be  
203 resolved with ICESat-2, as in Lake Eyre (Figure 1, SI1). In deriving the Lake Eyre bathymetry, we used at least four  
204 scans for each sub-basin, yielding an error of only 0.2-0.6 m (Table 1, Figure S4).

205 Another limitation to our methodology comes from the maximum water penetration of the ICESat-2 laser. This  
206 limits the ability to derive bathymetry in lakes that have a water depth of tens of meters or more. In such  
207 circumstances, a partial bathymetry could still be derived for the outskirts of the lakes using our methodology, or as  
208 presented in Li et al. (2019) or in Ma et al. (2019) for the shoulders of Lake Mead. However, we focus here on  
209 shallow desert lakes, in which, by definition, this is not a major obstacle.  
210 Sediment deposition could also increase the uncertainty of the derived bathymetry. Here, we use satellite imaging  
211 water occurrence from >30-yr period (Pekel et al., 2016), implying that if the lake floor was altered during this time  
212 interval, present-day ICESat-2 scans can yield only an averaged bathymetry of this period. However, newer global  
213 water occurrence datasets could emerge in the near future, enabling both derivation of newer bathymetries, and  
214 higher resolution maps (e.g., 10-20 m pixels from Sentinel-2).  
215 Apart from these limitations, taking a long series of satellite imagery extends a great opportunity. If only specific  
216 dates are used to identify isobaths (or shorelines), the error propagates to the bathymetric map. Using statistics based  
217 on many years, single image errors diminish. Such errors include water piling-up on one side of the lake due to  
218 winds (Arsen et al., 2013), misclassification of water boundaries or crossing isobaths (Long et al., 2019), and  
219 specific date imaging having only partial coverage of a lake, because of imaging geometry or cloud obscuration.  
220 Moreover, the use of specific date imagery requires a spatial interpolation between isobaths, thus concealing small  
221 features in between isobaths.  
222 Out of the three lakes analyzed above, Lake Eyre is probably the most closely monitored, yet the nearest river gauge  
223 is situated many hundreds of kilometers upstream. Therefore, there is no accurate in-situ data for water input  
224 volumes. ICESat-2's high spatial resolution (~70 cm) combined with high-resolution water occurrence map (e.g., 30  
225 m in the map of Pekel et al., 2016) yields an accurate, high-resolution bathymetry, even over flooded or complex  
226 desert lakes. Such maps could help in determining the water discharge into remote desert lakes and their evaporative  
227 losses, providing much-needed data in remote areas, serving as a basis for mass and energy balance calculations  
228 over such lakes, and for water management strategies.

## 229 **6 Conclusions**

230 Using a new methodology which links long-term water occurrence and accurate height measurements, each  
231 independently derived from satellite remote-sensing, we mapped the bathymetry of three shallow lakes in drylands  
232 across the globe. We verified the bathymetries using a previous bathymetric map, SRTM data, and through cross-  
233 validation. This easy-to-implement methodology yields a high-resolution bathymetry of shallow desert lakes that  
234 were flooded sometime during 1984-2015, using globally available datasets.

- 235 - As an example of a complex shallow lake system, we used Lake Eyre, consisting of multiple sub-basins.  
236 Despite its complexity, verification versus the best available DEM showed that the methodology is  
237 successful, as long as each sub-basin is covered by an elevation measurement scan.
- 238 - The methodology was also applied to two lakes with no previous bathymetry maps, one in the Sahara  
239 (Sabkhat El-Mellah) and the other in the Altiplano (Lago Coipasa). Results proved low cross-validation  
240 RMSD values (~0.3 m) compared with the SRTM data (~2.5 m).
- 241 - Applying the methodology in Lago Coipasa separately to “dry” and to “wet” ICESat-2 scans, relying on  
242 laser penetrability, we showed that bathymetry can even be produced during lake inundation.

243 The presented methodology can be applied to a large portion of the shallow lakes around the globe. It enables  
244 mapping of inundated lakes (a major obstacle for widely used methods), small lakes, and large and complex lake  
245 systems.

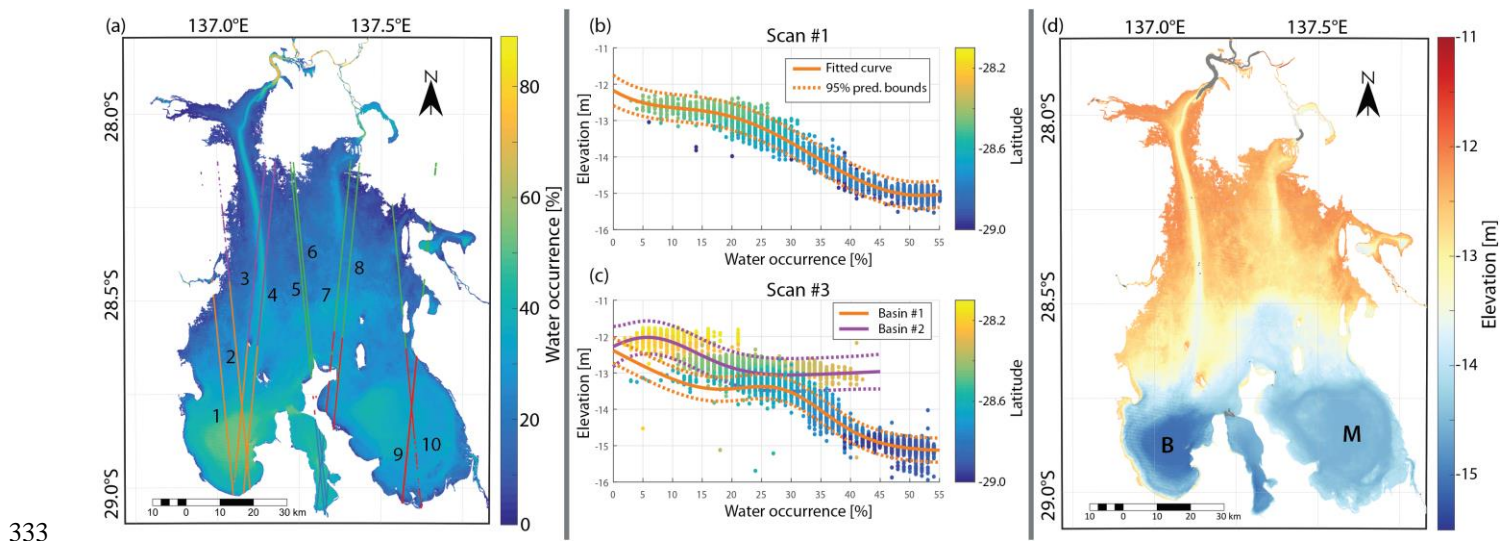
## 246 **Acknowledgments and Data**

247 This research was supported by ISF grant 946/18 and NSFC-ISF grant 2487/17 to YE. Water occurrence data (Pekel  
248 et al., 2016) were obtained from <https://global-surface-water.appspot.com>, using Google Earth Engine  
249 (<https://earthengine.google.com/>). ICESat-2 ATL03 data were obtained from <https://openaltimetry.org/data/icesat2/>;  
250 Neumann, T. A., A. Brenner, D. Hancock, J. Robbins, J. Saba, K. Harbeck, and A. Gibbons. 2019. ATLAS/ICESat-  
251 2 L2A Global Geolocated Photon Data, V1. [ATL03]. Boulder, Colorado USA. NSIDC: National Snow and Ice  
252 Data Center. doi: <https://doi.org/10.5067/ATLAS/ATL03.001>. [Dec 2019]. The authors declare no conflict of  
253 interests.

254 **References**

- 255 Arsen, A., Crétaux, J. F., Berge-Nguyen, M. and del Rio, R. A.: Remote sensing-derived bathymetry of Lake Poopó,  
 256 Remote Sens., 6(1), 407–420, doi:10.3390/rs6010407, 2013.
- 257 Berry, P. A. M., Garlick, J. D. and Smith, R. G.: Near-global validation of the SRTM DEM using satellite radar  
 258 altimetry, Remote Sens. Environ., 106(1), 17–27, doi:10.1016/j.rse.2006.07.011, 2007.
- 259 Brenner, A. C., DiMarzio, J. P. and Zwally, H. J.: Precision and accuracy of satellite radar and laser altimeter data  
 260 over the continental ice sheets, IEEE Trans. Geosci. Remote Sens., 45(2), 321–331,  
 261 doi:10.1109/TGRS.2006.887172, 2007.
- 262 Brunt, K. M., Neumann, T. A. and Smith, B. E.: Assessment of ICESat-2 Ice Sheet Surface Heights, Based on  
 263 Comparisons Over the Interior of the Antarctic Ice Sheet, Geophys. Res. Lett., 46, 13072–13078,  
 264 doi:10.1029/2019GL084886, 2019.
- 265 Bye, J. A. T., Dillon, P. J., Vandenberg, J. C. and Will, G. D.: Bathymetry of Lake Eyre, Trans. R. Soc. South Aust.,  
 266 102(1), 85–89, doi:10.1080/00359196009519029, 1978.
- 267 Cohen, T. J., Jansen, J. D., Gliganic, L. A., Larsen, J. R., Nanson, G. C., May, J. H., Jones, B. G. and Price, D. M.:  
 268 Hydrological transformation coincided with megafaunal extinction in central Australia, Geology, 43(3), 195–198,  
 269 doi:10.1130/G36346.1, 2015.
- 270 Cohen, T. J., Meyer, M. C. and May, J. H.: Identifying extreme pluvials in the last millennia using optical dating of  
 271 single grains of quartz from shorelines on Australia’s largest lake, Holocene, 28(1), 150–165,  
 272 doi:10.1177/0959683617715700, 2018.
- 273 Crétaux, J. F., Abarca-del-Río, R., Bergé-Nguyen, M., Arsen, A., Drolon, V., Clos, G. and Maisongrande, P.: Lake  
 274 Volume Monitoring from Space, Surv. Geophys., 37(2), 269–305, doi:10.1007/s10712-016-9362-6, 2016.
- 275 D’Odorico, P. and Porporato, A.: Dryland ecohydrology., 2006.
- 276 Enzel, Y. and Wells, S. G.: Extracting Holocene paleohydrology and paleoclimatology information from modern  
 277 extreme flood events: An example from southern California, Geomorphology, 19(3–4), 203–226,  
 278 doi:10.1016/s0169-555x(97)00015-9, 1997.
- 279 Feng, L., Hu, C., Chen, X., Li, R., Tian, L. and Murch, B.: MODIS observations of the bottom topography and its  
 280 inter-annual variability of Poyang Lake, Remote Sens. Environ., 115(10), 2729–2741,  
 281 doi:10.1016/j.rse.2011.06.013, 2011.
- 282 Forfinski-Sarkozi, N. A. and Parrish, C. E.: Analysis of MABEL bathymetry in Keweenaw Bay and implications for  
 283 ICESat-2 ATLAS, Remote Sens., 8(9), doi:10.3390/rs8090772, 2016.
- 284 Gao, H.: Satellite remote sensing of large lakes and reservoirs: from elevation and area to storage, Wiley Interdiscip.  
 285 Rev. Water, 2(2), 147–157, doi:10.1002/wat2.1065, 2015.
- 286 Jasinski, M. F., Stoll, J. D., Cook, W. B., Ondrusek, M., Stengel, E. and Brunt, K.: Inland and Near-Shore Water  
 287 Profiles Derived from the High-Altitude Multiple Altimeter Beam Experimental Lidar (MABEL), J. Coast. Res., 76,  
 288 44–55, doi:10.2112/si76-005, 2016.
- 289 Jawak, S. D., Vadlamani, S. S. and Luis, A. J.: A Synoptic Review on Deriving Bathymetry Information Using  
 290 Remote Sensing Technologies: Models, Methods and Comparisons, Adv. Remote Sens., 04(02), 147–162,  
 291 doi:10.4236/ars.2015.42013, 2015.
- 292 Kotwicki, V. and Isdale, P.: Hydrology of Lake Eyre, Australia: El Niño link, Palaeogeogr. Palaeoclimatol.  
 293 Palaeoecol., 84(1–4), 87–98, doi:10.1016/0031-0182(91)90037-R, 1991.
- 294 Leon, J. X. and Cohen, T. J.: An improved bathymetric model for the modern and palaeo Lake Eyre,  
 295 Geomorphology, 173–174, 69–79, doi:10.1016/j.geomorph.2012.05.029, 2012.
- 296 Li, Y., Gao, H., Jasinski, M. F., Zhang, S. and Stoll, J. D.: Deriving High-Resolution Reservoir Bathymetry From  
 297 ICESat-2 Prototype Photon-Counting Lidar and Landsat Imagery, IEEE Trans. Geosci. Remote Sens., PP(June), 1–  
 298 11, doi:10.1109/tgrs.2019.2917012, 2019.
- 299 Long, Y., Yan, S., Jiang, C., Wu, C., Tang, R. and Hu, S.: Inversion of Lake Bathymetry through Integrating Multi-  
 300 Temporal Landsat and ICESat Imagery, Sensors, 19(13), 2896, doi:10.3390/s19132896, 2019.
- 301 Ma, Y., Xu, N., Sun, J., Wang, X. H., Yang, F. and Li, S.: Estimating water levels and volumes of lakes dated back  
 302 to the 1980s using Landsat imagery and photon-counting lidar datasets, Remote Sens. Environ., 232(July), 111287,  
 303 doi:10.1016/j.rse.2019.111287, 2019.
- 304 Mabbutt, J. A.: Desert landforms, Second pri., The MIT Press, Cambridge, Massachusetts, USA., 1977.
- 305 Markus, T., Neumann, T., Martino, A., Abdalati, W., Brunt, K., Csatho, B., Farrell, S., Fricker, H., Gardner, A.,  
 306 Harding, D., Jasinski, M., Kwok, R., Magruder, L., Lubin, D., Luthcke, S., Morison, J., Nelson, R.,  
 307 Neuenschwander, A., Palm, S., Popescu, S., Shum, C. K., Schutz, B. E., Smith, B., Yang, Y. and Zwally, J.: The Ice,  
 308 Cloud, and land Elevation Satellite-2 (ICESat-2): Science requirements, concept, and implementation, Remote Sens.

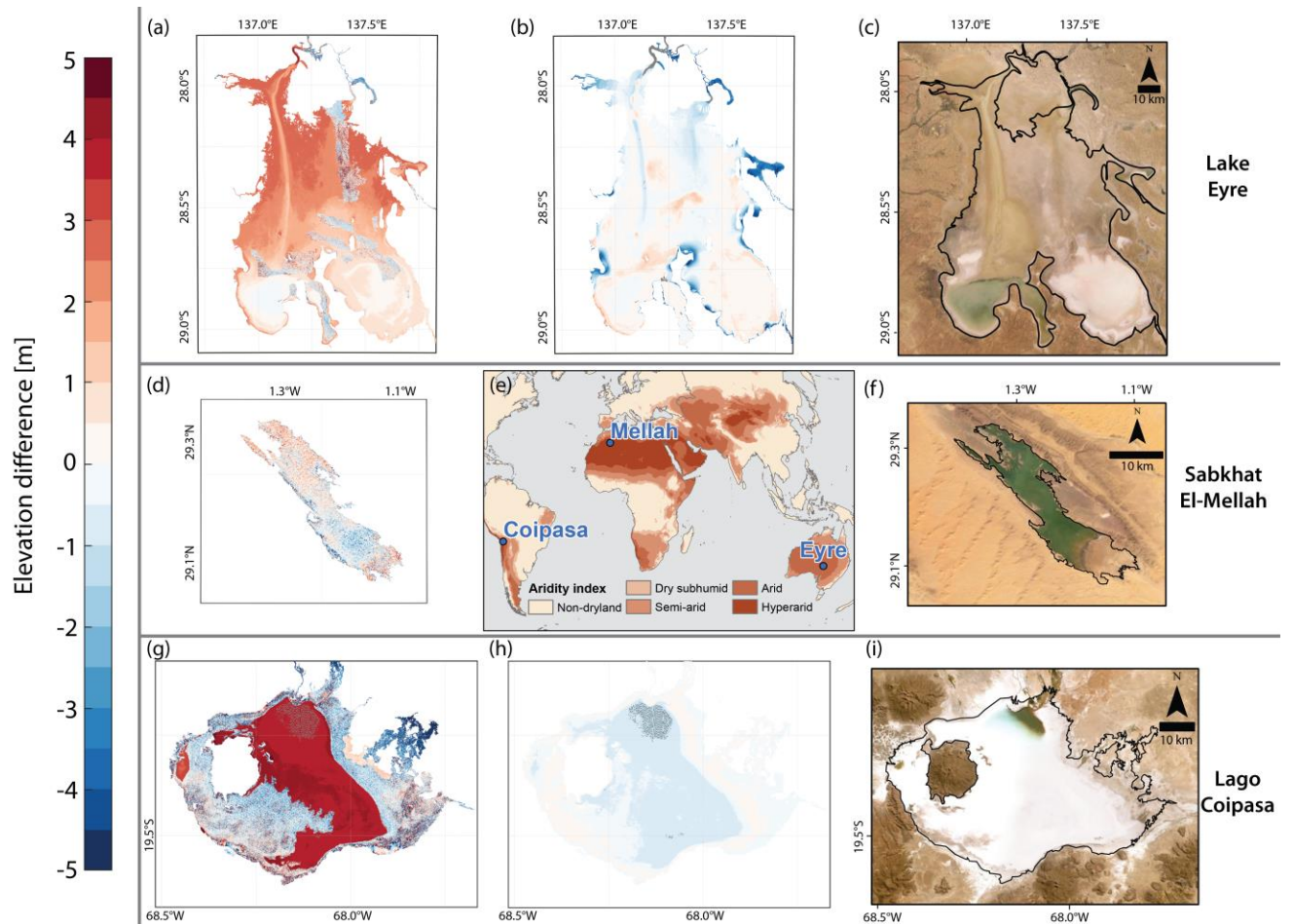
- 309 Environ., 190, 260–273, doi:10.1016/j.rse.2016.12.029, 2017.
- 310 de Martonne, E.: Regions of Interior-Basin Drainage, *Geogr. Rev.*, 17(3), 397–414, 1927.
- 311 New, M., Lister, D., Hulme, M. and Makin, I.: A high-resolution data set of surface climate over global land areas,  
312 *Clim. Res.*, 21(1), 1–25, doi:10.3354/cr021001, 2002.
- 313 Nicholson, S. E.: *Dryland climatology*, Cambridge University Press, New York., 2011.
- 314 Noy-Meir, I.: Desert Ecosystems: Environment and Producers, *Annu. Rev. Ecol. Syst.*, 4, 25–51, 1973.
- 315 Parrish, C. E., Magruder, L. A., Neuenchwander, A. L., Forfinski-Sarkozi, N., Alonzo, M. and Jasinski, M.:  
316 Validation of ICESat-2 ATLAS Bathymetry and Analysis of ATLAS’s Bathymetric Mapping Performance, *Remote*  
317 *Sens.*, 11(14), 1634, doi:10.3390/rs11141634, 2019.
- 318 Pekel, J. F., Cottam, A., Gorelick, N. and Belward, A. S.: High-resolution mapping of global surface water and its  
319 long-term changes, *Nature*, 540(7633), 418–422, doi:10.1038/nature20584, 2016.
- 320 Placzek, C., Quade, J. and Patchett, P. J.: Geochronology and stratigraphy of late Pleistocene lake cycles on the  
321 southern Bolivian Altiplano: Implications for causes of tropical climate change, *Bull. Geol. Soc. Am.*, 118(5–6),  
322 515–532, doi:10.1130/B25770.1, 2006.
- 323 Quade, J., Dente, E., Armon, M., Ben Dor, Y., Morin, E., Adam, O. and Enzel, Y.: Megalakes in the Sahara? A  
324 Review, *Quat. Res. (United States)*, 90(2), 253–275, doi:10.1017/qua.2018.46, 2018.
- 325 Schwanghart, W. and Scherler, D.: Short Communication: TopoToolbox 2 - MATLAB-based software for  
326 topographic analysis and modeling in Earth surface sciences, *Earth Surf. Dyn.*, 2(1), 1–7, doi:10.5194/esurf-2-1-  
327 2014, 2014.
- 328 Sun, F. and Ma, R.: Hydrologic changes of Aral Sea: A reveal by the combination of radar altimeter data and optical  
329 images, *Ann. GIS*, 25(3), 247–261, doi:10.1080/19475683.2019.1626909, 2019.
- 330 UNEP: *World atlas of desertification*, London : Edward Arnold, London., 1992.
- 331

332 **Figures and table**

334 **Figure 1.** An example of bathymetry derivation in Lake Eyre North (a schematic representation  
 335 of this process is in Fig S1). (a) Water occurrence from Pekel et al. (2016) and ten ICESat-2  
 336 scans over the lake (labeled) used to derive elevations. Scans are colored by the 5 identified  
 337 pseudo-watersheds (SI1). (b) The relation between water occurrence and elevation measurements  
 338 from ICESat-2 scan #1 with a two-term gaussian fit and its 95% prediction boundaries. Colors  
 339 represent latitude. (c) The same as in b, but for scan #3. The fit here is divided according to the  
 340 watersheds. (d) Derived bathymetry map based on the methodology presented in Section 2. Gray  
 341 dots represent regions in which water occurrence is greater than the highest occurrence  
 342 overpassed by ICESat-2. B = Belt Bay. M = Madigan Gulf.

343

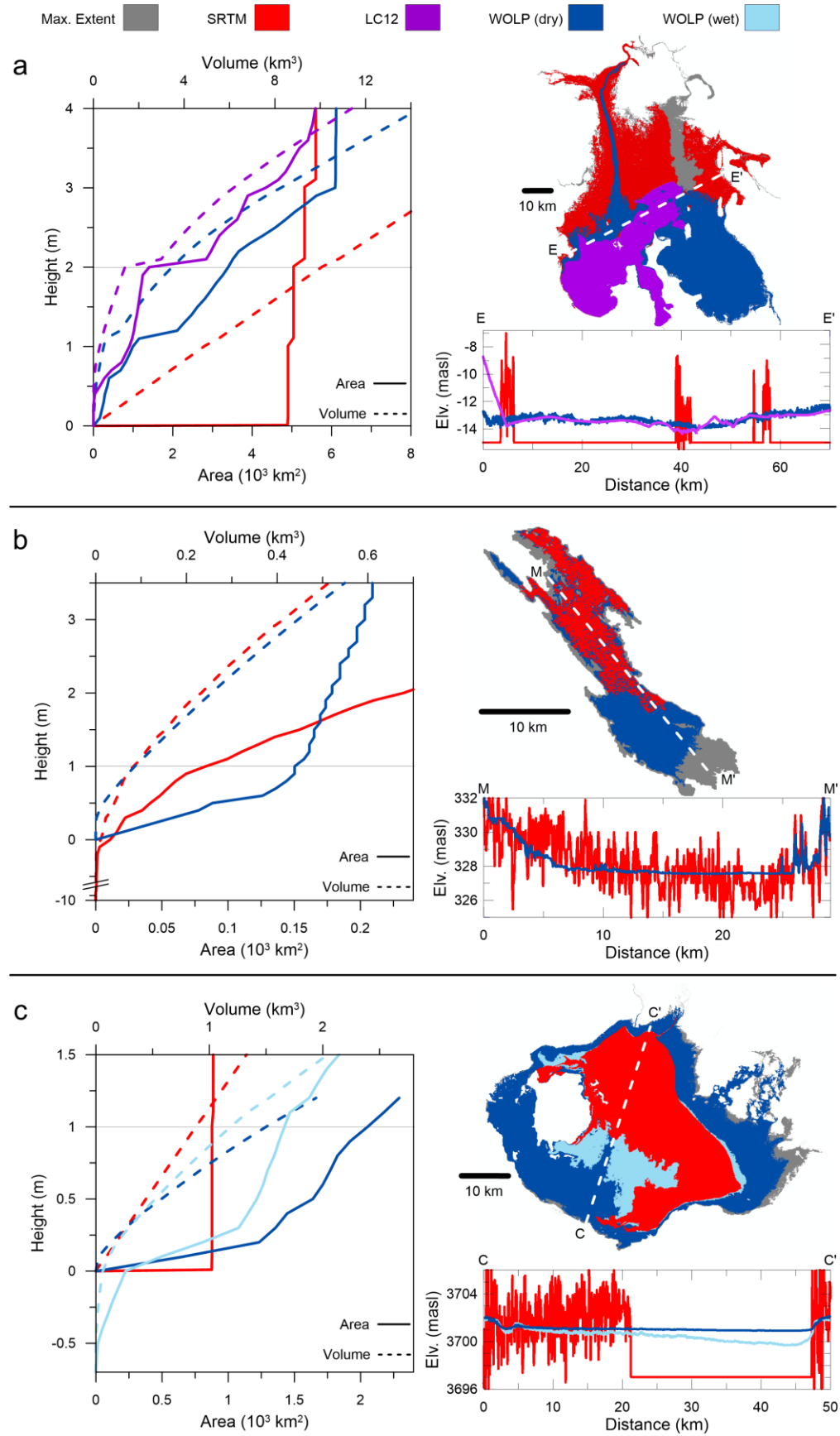
344



345

346 **Figure 2.** Comparisons of WOLP bathymetries with SRTM data in Lake Eyre (a), Sabkhat El-  
 347 Mellah (d), and Lago Coipasa (g). (b) Comparison of Lake Eyre bathymetry with the map of  
 348 Leon & Cohen (2012). (e) Location map of the three lakes, and aridity index (UNEP, 1992) from  
 349 the Climatic Research Unit of the University of East Anglia (New et al., 2002). True-color  
 350 satellite imagery of the lakes from Esri\Digitalglobe, and maximum extent of water occurrence in  
 351 black) from Pekel et al. (2016) (c, f, i). (h) Difference between the "wet" and "dry" bathymetries  
 352 of Lago Coipasa.

353



355 **Figure 3.** Hypsometric curves, extent maps and cross-sections for Lake Eyre (a), Sabkhat El-  
356 Mellah (b), and Lago Coipasa (c). The maps show filling extent at heights (denoted by a gray  
357 line on the hypsometric curves) that exert major differences between bathymetries. Details of the  
358 preparation of the hypsometries are in SI2.  
359

360

**Table 1.** *Validation results across the lakes*

Lake	Validated map	Reference	Regional / Profile validation	RMSD [m]	Lake depth [m]
Lake Eyre	SRTM	LC12	Regional	1.77	3.2 (WOLP) <sup>§</sup> , 4.1 (LC12) <sup>§</sup>
	WOLP (this study)	LC12	Regional	0.52	
	SRTM	ICESat-2	Profile	0.95-2.30*	
	LC12	ICESat-2	Profile	0.20-0.69*	
	WOLP	ICESat-2	Profile, cross-validation	0.21-0.57*	
Sabkhat El-Mellah	SRTM	ICESat-2	Profile	2.04 <sup>#</sup>	5.0 (WOLP) <sup>§</sup>
	WOLP	ICESat-2	Profile, cross-validation	0.32 <sup>#</sup>	
Lago Coipasa	SRTM	ICESat-2	Profile	2.84 <sup>#</sup>	1.2 (WOLP: “dry”) <sup>§</sup>
	WOLP (“dry”)	ICESat-2	Profile, cross-validation	0.28 <sup>#</sup>	
	WOLP (“wet”)	WOLP (“dry”)	Regional	0.39	2.2 (WOLP: “wet”) <sup>§</sup>
	WOLP (“wet”)	ICESat-2	Profile, cross-validation	0.47 <sup>#</sup>	

361 \*Range denotes the average RMSD for each sub-basin, averaged between the different ICESat-2 profiles in it.

362 <sup>#</sup>Average among the different ICESat-2 profiles.363 <sup>§</sup>Estimated (see SI2).

364